JGS
Journal of the Geological Society

Research article

Published online July 12, 2018 https://doi.org/10.1144/jgs2018-017 | Vol. 175 | 2018 | pp. 774–787

# Eocene ultra-high temperature (UHT) metamorphism in the Gruf complex (Central Alps): constraints by LA-ICPMS zircon and monazite dating in petrographic context


**Christian Nicollet[1]*, Valérie Bosse[1], Maria Iole Spalla[2] & Federica Schiavi[1]**

[1] Laboratoire Magmas et Volcans, Université Clermont Auvergne, CNRS, IRD, OPGC, F-63000 Clermont-Ferrand, France
[2] Dipartimento di Scienze della Terra 'A. Desio', Università degli Studi di Milano, Via Mangiagalli 34, 20133 Milan, Italy
M.I.S., 0000-0001-8346-5070
* Correspondence: christian.nicollet@uca.fr

**Abstract:** The Gruf complex in the Lepontine Alps is one of the rare occurrences of Phanerozoic ultra-high temperature (UHT) metamorphism in the world, but its age is still a matter of debate. Here we present LA-ICPMS dating in a petrographic context of zircon and monazite from a UHT restitic granulite. Zircons and monazites are both included in large crystals and in retrograde symplectites. In such restitic rocks, partial melting or fluid interactions are unlikely, precluding resetting of the monazite chronometers. Zircon cores yield Permian ages, which are interpreted as the age of charnockitization. They are sometimes surrounded by a narrow rim at 32 Ma. Monazites are strongly zoned, but all yield a 31.8 ± 0.3 Ma age interpreted as the time of complete (re-)crystallization during the UHT paragenesis. We propose that the zircons dated a post-Hercynian metamorphism which is responsible for the widespread formation of granulites in the Southern Alps and the crust differentiation. This fluid-absent melting event produced refractory lithologies, such as restites in charnockites. We suggest that Gruf UHT paragenesis is alpine in age and crystallized from these refractory lithologies. We conclude that the lower restitic crust produced in the Permian had the ability to achieve UHT conditions during the fast exhumation and heating related to lithospheric thinning in Alpine time.

**Supplementary material:** Analytical procedures for monazite analysis and dating, plus details of the major elements of the minerals, isotope data and trace element measurements in zircon are available at https://doi.org/10.6084/m9.figshare.c.4123619

**Received** 25 January 2018; **revised** 10 May 2018; **accepted** 1 June 2018

The Gruf complex in the Lepontine Alps is one of the rare occurrences of Phanerozoic ultra-high temperature (UHT) metamorphism in the world, discovered in the Val Codera by Cornelius (1916), Cornelius & Dittler (1929), and described by Barker (1964) and Wenk *et al.* (1974). Because occurrences of UHT metamorphism are mainly of Precambrian age (e.g. Harley 1998; Brown 2007; Kelsey & Hand 2015), this area is of major interest for understanding the geodynamic significance of such extreme metamorphic conditions. Indeed, the main difficulty in understanding the geodynamic significance of UHT metamorphism is that Precambrian UHT granulites are often preserved in small-scale lenses: they usually represent structural and metamorphic relicts in polymetamorphic rocks belonging to polycyclic terrains. The lack of large-scale tectonic structures associated with their emplacement precludes a clear understanding of their geodynamic history. Therefore, the few Phanerozoic UHT occurrences for which the geological context is well constrained are precious records that help us to understand and interpret this type of metamorphism.

The age of the UHT metamorphism in the Gruf complex is currently a matter of debate. Based on zircon U–Pb dating, Galli *et al.* (2012) proposed a Permian age (282–260 Ma) for the granulite facies fluid-absent biotite melting event. For these authors, the presence of orthopyroxene inclusions in zircons confirms the Permian age of the charnockites and associated sapphirine-bearing granulites. Zircon rims from the same samples yield ages of 34–29 Ma, interpreted as dating the Alpine amphibolite-facies migmatization. A different interpretation was suggested by Droop & Bucher-Nurminen (1984) and proposed by Liati & Gebauer (2003). The latter authors considered that the zircon Alpine rims (yielding a weighted mean age of 32.7 ± 0.5 Ma in their samples) grew during the UHT metamorphic event, and that the sapphirine-bearing granulites were restites formed during partial melting of the Permian granitoids. Moreover, Schmitz *et al.* (2009), measuring an age of 33.0 ± 4.4 Ma by monazite chemical dating also agree with this interpretation.

These contrasting results imply two different models for the origin of the UHT metamorphism.

(1) A Permian UHT metamorphism can be linked to the post-Hercynian high-thermal regime, associated with lithospheric Permian–Triassic thinning and responsible for the widespread formation of granulites in the Austroalpine and South-Alpine continental crust (e.g. Brodie *et al.* 1989; Lardeaux & Spalla 1991; Diella *et al.* 1992; Barboza & Bergantz 2000; Müntener *et al.* 2000; Schuster *et al.* 2001; Spalla & Marotta 2007; Schuster & Stuewe 2008; Galli *et al.*, 2013; Spalla *et al.* 2014). This anomalously high thermal regime would be responsible for a pervasive melting event, associated with melt loss leading to the genesis of a residual, refractory lower crust. Such processes are interpreted as being responsible for differentiation of the lower continental crust (e.g. Vielzeuf & Holloway 1988; Brown 2008; Redler *et al.* 2013).

(2) An Alpine UHT metamorphism would have been driven by lithospheric thinning associated with slab breakoff and asthenospheric upwelling (e.g. Davies & Von Blanckenburg 1995; Von Blanckenburg & Davies 1995; Oalmann *et al.* 2016), which would provide the considerable amount of heat necessary to reach the UHT conditions.

In this study, we combine for the first time zircon and monazite *in situ* dating in a petrographic context for the Gruf sapphirine-bearing

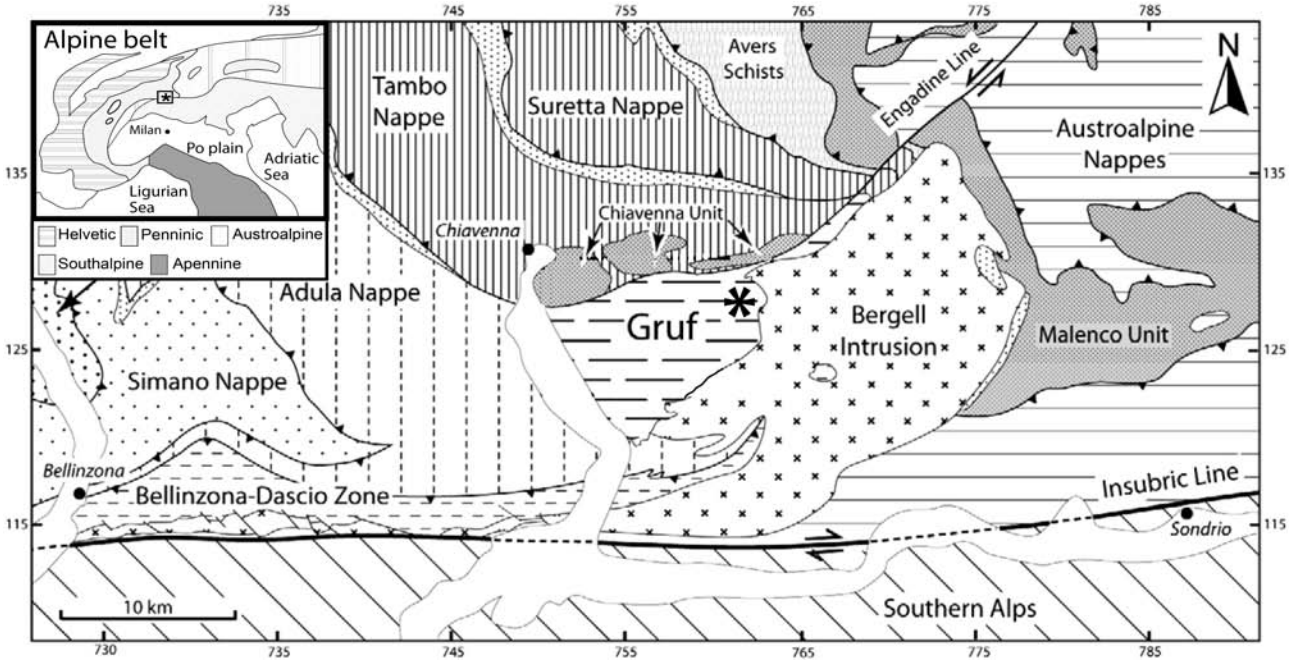


**Fig. 1.** Sketch map of the Gruf complex in the eastern Central Alps after Galli *et al.* (2011). Asterisk locates upper Val Codera. The sketch is located in the Alpine chain (inset).

granulite. The results provide a new opportunity to clarify the age of the UHT event and its geodynamic context.

## Geological setting

Penninic nappes in the Central Alps consist of variegated rocks of continental and oceanic origins. This nappe stack is separated from the Southern Alps by the Periadriatic Lineament and by a thin ribbon of Austroalpine crust verticalized along the 'southern steep belt' (e.g. Schmid *et al.* 1996). The axial portion of the Central Alps has recorded a polycyclic metamorphic evolution: structural and petrological relicts of Hercynian and Caledonian imprints have been described (Schaltegger 1994; Spalla *et al.* 2014 and references therein). The Alpine overprint occurs with heterogeneous intensity and, for some time, it has been difficult to separate the Alpine from the pre-Alpine metamorphic imprints due to the similar metamorphic conditions associated with these successive orogenic cycles (e.g. Niggli 1974; Engi *et al.* 2004). Alpine metamorphism in the Central Alps is characterized by a polyphasic metamorphic evolution characterized by an early high pressure–low- to intermediate-temperature imprint, preserved as relict blueschist- and eclogite-facies assemblages, recorded during the south-verging subduction. The second metamorphic imprint is characterized by assemblages indicating a Barrow-type event interpreted as consequent to the continental collision. Isograds of the Barrovian metamorphism define the 'Lepontine metamorphic dome' (Trommsdorff 1966; Todd & Engi 1997) and their concentric distribution indicates that metamorphic conditions increase southwards from greenschist- to upper amphibolite-facies. In this southern part, partial melting conditions have been attained at about 700°C and 0.6-0.8 GPa between 32 and 22 Ma (Engi *et al.* 1995; Burri *et al.* 2005; Berger *et al.* 2009; Rubatto *et al.* 2009). The Gruf complex (Fig. 1) is a small tectonic unit of about 200 km$^2$, located in the southeastern part of the Lepontine dome, north of the Insubric Line, and limited to the east by the calc-alkaline Tertiary intrusive stock of Bergell. This intrusive massif is considered synchronous with crustal anatexis at 33–28 Ma (Berger *et al.* 1996). The Gruf complex is composed mainly of biotite–garnet–sillimanite–cordierite metapelitic rocks and migmatitic orthogneisses and paragneisses, and has been recently considered as part of the tectonic mélange of continental and oceanic units accreted together in the Alpine tectonic accretion channel (Engi *et al.* 2001). During remarkable field work in very difficult terrain, Galli *et al.* (2012) described structural and petrological characters of the complex *in situ* for the first time, focusing especially on the Mg–Al-rich sapphirine granulites. The latter form schlieren and residual enclaves within sheet-like bodies of charnockites and migmatitic orthogneisses (Galli *et al.* 2013). The chemical composition of the Mg–Al-rich granulites is comparable with that of restitic surmicaceous enclaves in granites (e.g. Montel *et al.* 1991) except for magnesium. Kelsey *et al.* (2003) suggested that the production of Mg–Al-rich compositions through melt loss is improbable because of the low Mg partition into melt. For these authors Mg-rich assemblages may source from Mg-enriched protoliths. Consequently, the Gruf Mg–Al-rich sapphirine granulites may represent resister lenses (which resist migmatisation by virtue of their unsuitable compositions (McLellan, 1989)) within charnockites/orthogneisses or restites from Mg-rich protolith included in the charnockites.

Previously published geochronological studies are at the origin of the contrasted interpretations for the geodynamic significance of the UHT conditions recorded in the Gruf complex. Liati & Gebauer (2003) report SHRIMP weighted mean ages of 272.0 ± 4.1 Ma in zircon cores and of 32.7 ± 0.5 Ma in zircon rims from a sapphirine-bearing granulite sample. The Permian ages are interpreted as reflecting the age of the magmatic protolith, whereas the Alpine ages are considered to represent the age of the granulite-facies metamorphism. For these authors, sapphirine-bearing granulites represent restites formed during Alpine partial melting of Permian granitoids. Galli *et al.* (2011, 2012) proposed a different interpretation based on similar geochronological data obtained with the same method (zircon SHRIMP analyses). For these authors 282–260 Ma ages obtained in oscillatory zoned zircon cores represent melts generated through granulite-facies fluid-absent biotite melting at 920–940°C in metapelitic rocks, whereas 34–29 Ma ages in zircon rims date the Alpine amphibolite-facies migmatization. For these authors the charnockites associated with the sapphirine-bearing granulites belong to the post-Hercynian European lower crust. Schmitz *et al.* (2009) applied 3D micro-X-ray fluorescence analysis to monazite in thin section from a sapphirine-

bearing granulite. They obtained an age of 33.0 ± 4.4 Ma in monazites included in and intergrown with high-temperature (HT) minerals which they interpreted as the age of the high-temperature event. Finally, Oalmann *et al.* (2013, 2016) also suggest that UHT conditions were reached slightly before 32.5 Ma followed by cooling from 30 to 19 Ma recorded by rutile $^{206}Pb/^{238}U$ ages.

## Petrography of the Mg–Al granulites

Mg–Al-rich sapphirine granulites have already been carefully described by Barker (1964), Droop & Bucher-Nurminen (1984), Galli *et al.* (2011) and Guevara & Caddick (2016). We will concentrate here on the main petrological characters and mineral reactions, which appear to be of major interest to link petrology and geochronology. The studied sample is a pebble which was collected in upper Val Codera (Fig. 1). Two domains have been recognized at the sample scale: one is a sapphirine-bearing granulite (Fig. 2a; three-quarters of the sample) while the other has the typical mineralogy of a charnockite (Fig. 2d, e; quarter of the sample). The boundary between these two domains is progressive. Composition of the granulitic domain is enigmatic. Galli *et al.* (2011) propose that the granulitic domain could be a restite/schlieren of Mg-rich metapelite. It could be a resister of an unknown (magnesian?) protolith within the charnockitic domain. The charnockitic paragenesis is composed of millimetric to pluri-millimetric crystals of Opx–Bt–Kfs ± Pl–Qz–Mnz–Zrn and Ap (Fig. 2d, e; abbreviations in text and figures are from Whitney & Evans (2010)). Rare inclusions of zircon, monazite, plagioclase and quartz are observed in the phenocrysts. In some places, clusters of K-feldspar–quartz–apatite microcrysts follow the grain boundaries in the charnockitic assemblage (Fig. 2e). They seem to represent incipient melting or residual melt after extraction. In the charnockite domain, K-feldspar is orthose (XOr: 80%; XAb: 20%), plagioclase has an intermediate composition with XAn: 40. The compositions of orthopyroxene and biotite are substantially the same as in the granulitic domain of the rock.

The primary crystals of the residual/resister granulite are millimetric to plurimillimetric in size. The peak UHT paragenesis was: Al-rich Opx–Sil–Spr–Bt–Grt–Crd–Rt–Ap–Zrn–Mnz (Fig. 2a). Here again some tiny inclusions are rarely present. Detailed observations of the mineral associations reveal complex relationships with (at least) two generations of Al-rich orthopyroxene, sillimanite, cordierite and sapphirine ± spinel ± biotite, garnet and rare inclusions of quartz, rutile and apatite. Secondary minerals are abundant. Except for orthopyroxene, the chemical composition of the minerals does not change much and the crystals are weakly zoned (Supplementary material table A). Garnet is almost pure almandine–pyrope solid solution with a slight decrease in pyrope relative to almandine at the rim of the crystals (from the core to the rim: XPy: 48–46%; XAlm: 42–45%). Grossular and spessartine contents are low: XGrs: 2.2–3.1% and XSp: ≤1%. Opx is $Al_2O_3$-rich and zoned (core: 7.5–8.6% and rim: 5.5–7% Fig. 3). Biotite is Mg- (XMg: 75–80%) and Ti-rich ($TiO_2$: 2.6–3.6%). Cordierite composition is homogeneous both in primary minerals and in symplectites. Galli *et al.* (2011), Oalmann *et al.* (2013) and Guevara & Caddick (2016) estimated the conditions of the primary paragenesis in these granulites at $T = 920–940°C$ and $P = 0.85–0.95$ GPa.

The secondary symplectites in the granulites are varied and complex, with Spr, Sil, Crd, Opx ± Sp. Spinel is hercynite–spinel solution, homogeneous in composition. Two main reactions dominate (Fig. 2b–c): Sil 1 phenocrysts are surrounded by Spr 2 + Crd 2 in contact with Opx ± Bt; the garnet is destabilized into symplectites of Opx 2 + Crd 2. These two reactions indicate a pressure decrease. $Al_2O_3$ content in Opx 2 is between 7.4 and 5.9%, similar to the rims of the primary phenocrysts (Fig. 3), whereas the XMg is slightly lower than in the primary crystals. Primary Opx probably continues to grow at the beginning of the retrograde evolution during decompression, while garnet is destabilized. This suggests that primary paragenesis and retrograde symplectites are the product of a single metamorphic event. These retrograde textures demonstrate a re-equilibration of the UHT peak assemblages at lower metamorphic conditions: 720–740°C at 6.5–7.5 kbar, which starts with a decompression and continues with a temperature decrease (Galli *et al.* 2011; Oalmann *et al.* 2013; Guevara & Caddick 2016). These conditions are similar to those inferred for the migmatization occurring during Tertiary Barrovian regional metamorphism (Engi *et al.* 1995; Burri *et al.* 2005).

Both zircons and monazites are included in the large crystals (namely primary phenocrysts): orthopyroxene, orthoclase from the charnockitic assemblage; sapphirine, orthopyroxene, sillimanite, cordierite from the UHT assemblage, as well as in the cordierite–biotite matrix and in the late symplectites. Mineral inclusions are rare in garnet and zircon and monazite have not been detected in it.

## Zircon and monazite textures

Zircons are subhedral, elongated and/or resorbed, rounded crystals 30–100 μm long. They contain rare and very tiny inclusions among which biotite, white mica, quartz and apatite were only unequivocally identified by Raman spectrometry. Sillimanite has not been observed. Zircons included in the primary phenocrysts of the two domains are resorbed grains and seem to be relictual (Fig. 4a). Cathodoluminescence images (CLI) show that most of the grains display a large inner domain with usually oscillatory or rarely complex zoning (Fig. 4b–c). In zircon included in the cordierite–biotite matrix and in late symplectites, this inner domain is sometimes surrounded by a thin rim (<5 μm to 15 μm) with euhedral faces and it is bright in CLI (Fig. 4c). U and Th contents are variable ($150 < U < \sim4860$ ppm and $4 < Th < 1180$ ppm; Supplementary material, table B) with no correlation with the internal structure or ages (see the next section). As a result, Th/U ratios are also variable ($0 < Th/U < 0.50$) and unrelated to the different zircon domains (i.e. oscillatory zoned inner domain or external rim). Trace elements have been analysed in the core and in the rims of the zircon grains. Because the rims are very thin compared to the spot size (15 μm), we were not able to properly analyse the rims. The rare earth element (REE) patterns of the zircons show an enriched distribution of heavy REE, negative Eu anomalies ($Eu/Eu^* = 0.05–0.09$) and positive Ce anomalies (see Supplementary material, table C), which are similar to those described in zircon from Grt-bearing granulite-facies rocks (Rubatto 2002). Zircons from the charnockite domain display he same REE pattern as those of granulite.

Monazites are 50 to 150 μm in size and are present in the core of large Spr, Opx, Crd crystals or form clusters of small grains (10–40 μm) in the late symplectites. The shape of the grains varies from large, rounded grains to small, elongated ones with rarely indented grain boundaries (Figs 5b and 6a), without any correlation with the textural position. Needles of sillimanite are rare inclusions (Fig. 6a). All the grains are strongly zoned (Table 1). Chemical variations of the light REE- (LREE-), Th- and Ca-contents broadly follow the brabantite substitution ($2REE^{3+} = Th^{4+} + Ca^{2+}$). $ThO_2$ content varies from 1.3 to 10.8 wt%. $Y_2O_3$ and $UO_2$ contents are highly variable (from 0.1 to 5.5 wt% and from 0.2 to 3.5 wt%, respectively) and inversely correlated. These variations are clearly related to mineral position within the sample (Fig. 7a): monazites in the charnockite domain are Y-rich and U-poor whereas the opposite is true in the granulite domain. Variations in LREE, MREE (middle rare earth elements) and $Y_2O_3$ contents are also correlated with the sample zonation: monazites from the charnockite domain are enriched in $Gd_2O_3$ and $Y_2O_3$ whereas monazites from the granulite domain are enriched in $La_2O_3$ and poor in $Gd_2O_3$ and $Y_2O_3$ (Fig. 7b–c). Chemical variations are observed from one grain to another but also within a single crystal: for example the T50M1

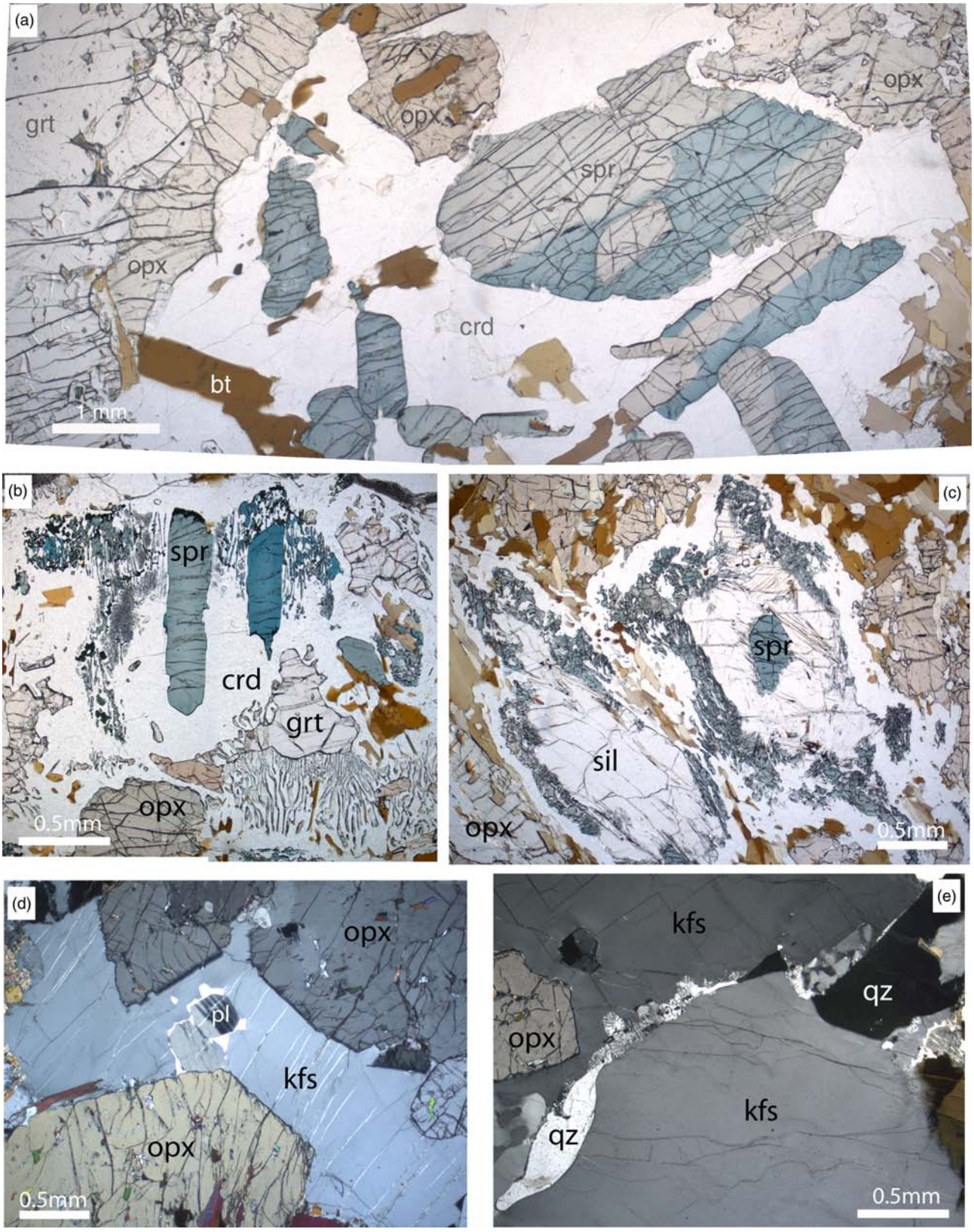


**Fig. 2.** Microphotographs of the parageneses and textures of the granulitic rock in plane- (PPL) and cross- (XPL) polarized light: (**a**) the Spr-bearing granulitic paragenesis (PPL); (**b**) complex retrograde symplectites in the Spr-bearing portion of the rock granulite with spr2, sp, cord, sil2. Opx + Crd symplectites replace Grt (PPL); (**c**) Spr2 + crd resulting from the retrograde reaction Opx + Sil = Spr + Crd (PPL); (**d**) the charnockitic paragenesis (XPL); (**e**) textures of incipient melting or residual melt after extraction in the charnockite portion of the rock (XPL). Abbreviations in text and figures are from Whitney & Evans (2010).

crystal in Figures 6a and 7 in the Al-granulite domain; T14M1 crystal in Figure 7 and T12M1 crystal in Figure 6b in the charnockite domain. Some of the grains display very tiny Y-rich overgrowths (Fig. 6a).

## U–Th–Pb geochronology

Monazite and zircon have been analysed in thin section by LA-ICPMS in order to control the position of the grain (and thus the

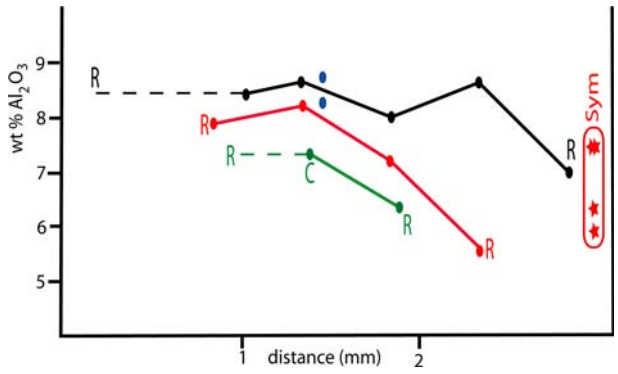


**Fig. 3.** $Al_2O_3$ profiles in the primary Opx (C denotes core and R denotes rim) and $Al_2O_3$ concentrations (contents values) in the Opx from the Opx + Crd symplectite (sym) around garnet.

measured ages) relative to the textures observed in the sample. Zircons and monazites were ablated using a Resonetics Resolution M-50 equipped with a 193 nm Excimer laser system coupled to an Agilent 7500 cs ICP-MS with a 1 Hz repetition rate, a fluence of 7 J $cm^{-2}$ and a spot size of 7 μm for monazite dating and 3 Hz repetition rate, a fluence of 2.6 J $cm^{-2}$ and a spot size of 20 μm for zircon dating. The helium carrier gas was supplemented with $N_2$ prior to mixing with Ar for sensitivity enhancement (Paquette *et al.* 2014). Detailed analytical procedures are reported in Paquette & Tiepolo (2007) and Didier *et al.* (2015) and in the Supplementary material. Monazite can be dated using both U–Pb and Th–Pb decay schemes. Here we will only consider $^{208}Pb/^{232}Th$ ages for the following reasons. Firstly, $^{232}Th$ is largely predominant in monazite, allowing small spots (7 μm) to be performed during laser ablation. Secondly, the U decay series could be in disequilibrium in young monazites (Schärer 1984), resulting in overestimated $^{206}Pb/^{238}U$ ages. Because secular equilibrium among the intermediate daughters of $^{232}Th$ occurs after about 30 years, it seems reasonable to assume that initial $^{208}Pb$ is absent. Thirdly, $^{232}Th$ is so abundant that $^{208}Pb$ originating from common Pb is usually negligible compared to radiogenic $^{208}Pb$. To reinforce this hypothesis, we only consider here the concordant $^{208}Pb/^{232}Th$–$^{206}Pb/^{238}U$ ages (Fig. 8a). Whatever the textural position of the monazite grains or the chemical composition of the monazite domain, the $^{208}Pb/^{232}Th$ ages are between 29.6 ± 1.0 and 34.1 ± 1.1 Ma, allowing us to calculate a weighted average age of 31.8 ± 0.3 Ma (MSWD = 3.2, $n$ = 51; Fig. 8b; Supplementary material, table B). Note the important chemical variations in the same crystal, but identical ages (Figs 6 and 7), suggesting significant chemical transfer and/or variation of the redox state through the rock during this brief metamorphic episode of UHT.

$^{206}Pb/^{238}U$ ages measured in zircon from our sample are scattered from 30 ± 1 to 304 ± 12 Ma (only U/Pb concordant ages; Fig. 8c). Ages are similar in the charnockite and granulite domains. The youngest ages were obtained in the bright rims. Plotted in a Tera Wasserburg diagram, we see that these ages are in total agreement with the ages measured in the monazite grains (Fig. 8c). The oldest ages are upper Carboniferous–lower Permian and were obtained in the inner oscillatory zoned domains. Two reasons can be provided to explain the intermediate ages between the oldest and the youngest ones: (i) they reflect mixing between the Carboniferous core and the narrow Cenozoic rim (<5 to 15 μm) due to analysis of distinct adjacent domains; (ii) they result from Pb loss. Indeed, in some of the grains the U content is high (U > 1000 ppm). Such a high U content could be responsible for radiation damage of the crystal lattice, especially in Paleozoic zircons and induce Pb loss. This results in a younger core compared to the rim, as observed in Figure 4b. With the aim of limiting these two effects and to better restrict the range of the oldest ages, we decide to consider only the ages which were measured (i) in the zircon crystals which do not present the luminescent rim on the CLI and (ii) measured in domains with U content ≤1000 ppm. By doing this the scattering of the $^{206}Pb/^{238}U$ ages remains between 247 ± 6 and 304 ± 12 Ma (Fig. 8d).

## Discussion

### *Ages recorded in zircon*

Two groups of ages were recorded in the zircons: between 247 ± 6 and 304 ± 12 Ma in the core and *c.* 30 Ma in the rim. These ages are in total agreement with the results obtained by Liati & Gebauer (2003) and Galli *et al.* (2012). Following these last authors, who found the charnockitic paragenesis included within the zircon cores, the ages measured in the oscillatory zoned inner domain could be interpreted as the age of the charnockitization. As no older inherited domains have been observed in our zircons, we favour this interpretation. This charnockitization can be developed under the Permian–Triassic high-thermal regime (Galli *et al.* 2013) responsible for the widespread formation of granulites in the Southern Alps and Austroalpine area (Bertotti *et al.* 1993; Spalla & Marotta 2007; Spalla *et al.* 2014 and references therein). The scattering of the ages between 247 and 304 Ma in a single sample is rather surprising and, as previously suggested, cannot only be attributed to mixing ages. Such a large spread of zircon ages is known in other Austroalpine and Southalpine units (Marotta *et al.* 2018 and references therein), representing lower continental crust: Ivrea zone (Vavra & Schaltegger 1999; Peressini *et al.* 2007), Malenco (Müntener *et al.* 2000), Sondalo (Tribuzio *et al.* 1999) and Valtournanche (Manzotti *et al.* 2012). Vavra & Schaltegger (1999) suggest that the U–Pb system in zircons from the Ivrea zone could have been disturbed by different types of alteration and Pb-loss processes during Permian, Triassic and possibly early Jurassic times. These perturbations were interpreted differently as consequent to the early stages of Mesozoic rifting related to thermal and/or decompression pulses during extensional unroofing in the Permian (Marotta *et al.* 2009), as, for example, in Valtournenche, where pre-Alpine evolution is associated with low pressure (LP)–HT metamorphism related to Permian–Triassic lithospheric thinning (Manzotti *et al.* 2012; Manzotti & Zucali 2013). Our results, although slightly older than the previously published ages (but within the 2σ error bar), are in agreement with these interpretations.

The second group of ages, between 30 ± 1 Ma and 34 ± 2 Ma, was recorded in euhedral rims from some crystals included in the Bt–Crd matrix or Spr–Crd symplectites. Most of the zircons included in the primary phenocrysts do not present such a younger rim (Fig. 4b). Furthermore, these results are similar to the $^{208}Pb/^{232}Th$ ages measured in the adjacent monazites, whatever the textural position of the latter. Thus, these results argue for a zircon recrystallization event at *c.* 32 Ma, concurrent with the crystallization (or re-crystallization, see the discussion below) of the monazite grains.

### *Monazite ages*

Contrary to the zircon results, monazites from the studied sample provide a narrow age estimation at 31.8 ± 0.3 Ma (between 29.6 ± 1.0 and 34.1 ± 1.1 Ma). The ages are the same in all the different textural positions of the monazite (included in large Spr, Opx or Crd crystals or in the Crd–Bt matrix or as cluster of small grains within secondary symplectites), or the chemical zoning or the granulitic (Fig. 6a) or charnockitic (Fig. 6b) paragenesis. The Y-rich overgrowths observed in some monazite grains, which could be related to garnet destabilization (Didier *et al.* 2014), do not yield younger ages (Fig. 6a). Similarly, no older ages (i.e. Paleozoic) have been recorded by the monazites. Usually the shape of the monazite grains suggests

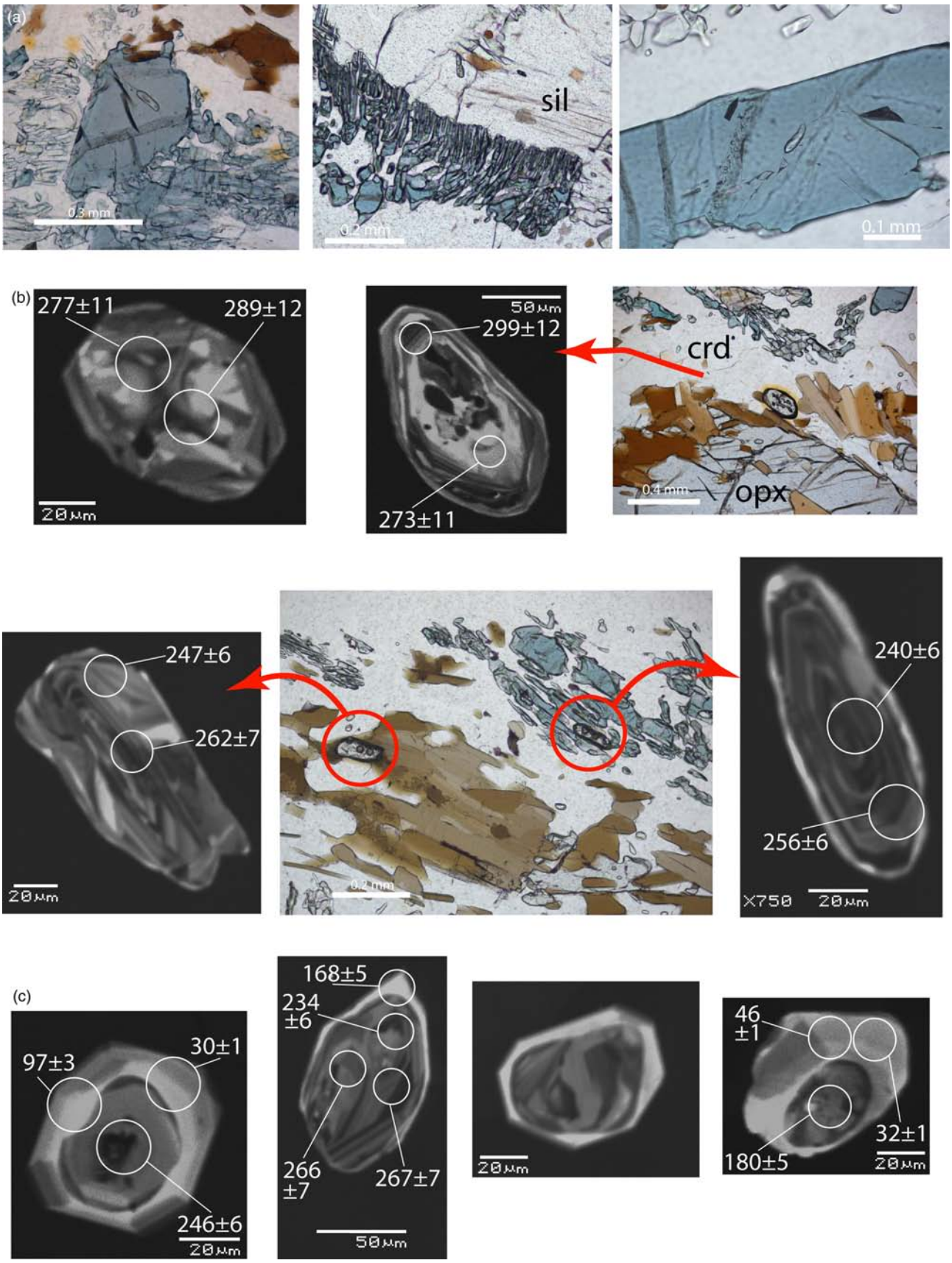


**Fig. 4.** (**a**) Resorbed crystals of zircons included in primary phenocrysts, Spr and Sil (PPL); (**b**) cathodoluminescence images of zircons in the Crd–Bt matrix with oscillatory zoning; (**c**) zircon grains surrounded by highly luminescent rim (<5–15 μm) with euhedral faces with Alpine or intermediate ages ($^{206}Pb/^{238}U$ ages; 2σ).

equilibrium with, on the one hand, the large primary crystals recording the peak of the UHT conditions and, on the other hand, with the secondary symplectites during the beginning of retrograde evolution. This demonstrates that the Spr–Opx–Sil UHT paragenesis, as well as the retrograde symplectites in the restitic granulites, equilibrated at *c.* 32 Ma, in agreement with earlier works (Droop &

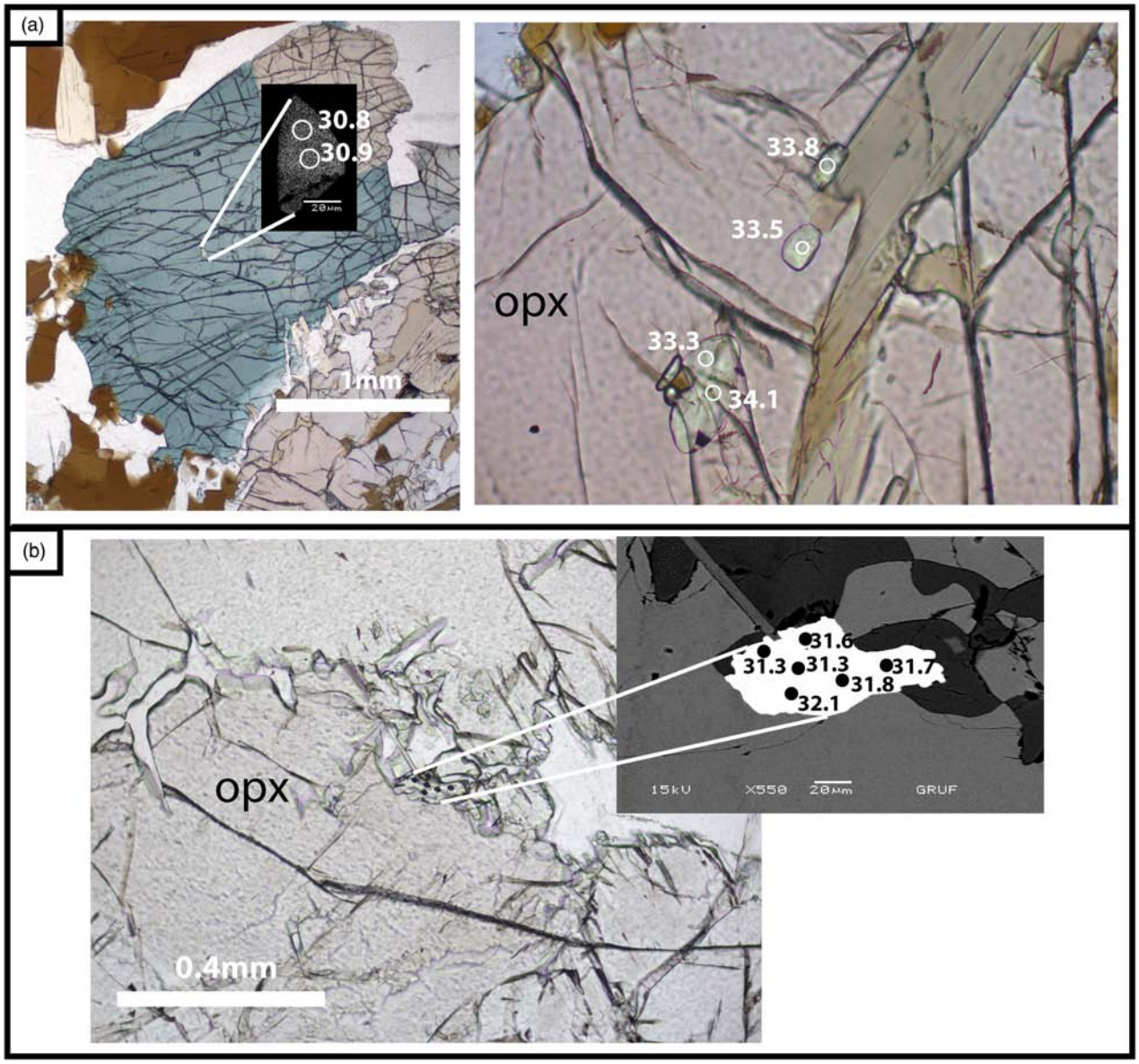


**Fig. 5.** (**a**) Monazite inclusions in the phenocrysts (PPL) of sapphirine and Al-rich orthopyroxene of the Spr-bearing domain of the rock. (**b**) Monazite inclusions in an Opx of the charnockite portion of the rock; note the tiny overgrowths (rich in Y) in the backscattered electron (BSE) image (crystal T14M1). Circles are $^{208}Pb/^{232}Th$ ages in Ma (with ±1.1 Ma for all data).

Bucher-Nurminen 1984; Liati & Gebauer 2003; Schmitz *et al.* 2009). The Alpine UHT event is recorded by the monazite and by the zircon rims.

### *Age of UHT metamorphism in the Gruf complex*

Our zircon and monazite age results point to an age of 32 Ma for UHT metamorphism. Galli *et al.* (2011, 2012, 2013) disagree with this interpretation. In their model, the Alpine age recorded in the zircon rims represents the age of the migmatization of the Gruf lithologies in the upper amphibolite-facies conditions. Moreover, they interpreted that the ages recorded as 33.0 ± 4.4 Ma by monazite (Schmitz *et al.* 2009) are supposedly the result of the monazite resetting during fluid-assisted migmatization (Galli *et al.* 2012). We cannot support this interpretation for two reasons. First, many examples exist in the literature that show that monazite is a robust geochronometer able to retain age records during anatectic processes (Paquette *et al.* 2004; Rubatto *et al.* 2006, 2013; Stepanov *et al.* 2012; Didier *et al.* 2014, 2015) or even UHT conditions (Korhonen *et al.* 2013; Rocha *et al.* 2017). The main causes of possible disturbance of the Th–U–Pb systems in monazite are dissolution/recrystallization processes during melt or hydrous fluid interaction (e.g. Cherniak *et al.* 2004; Kelly *et al.* 2012). Fluid interaction in the present context is difficult to argue and, in any case, supposes an external input (see the next point below). Dissolution/recrystallization processes during melt interaction strongly depend upon the melt composition and its $H_2O$ content (Montel 1986; Rapp & Watson 1986; Spear & Pyle 2002). Monazite solubility is low in meta- or peraluminous melts and thus monazite is able to resist to crustal anatexis. To conclude, if fluid-assisted migmatization in the amphibolite conditions occurred during Alpine times following a Permian UHT event, we would expect to measure Permian ages in part of the monazite domains or grains, which is not the case. 'Resetting' cannot be an explanation for the absence of Permian age records in monazite in the present conditions.

The second point questions the migmatization processes in such refractory lithologies. As reported by Galli *et al.* (2011), Mg–Al granulites occur as restites or schlieren in the charnockites and thus represent highly refractory rocks formed during partial melting processes in Permian times. Partial melting of such refractory

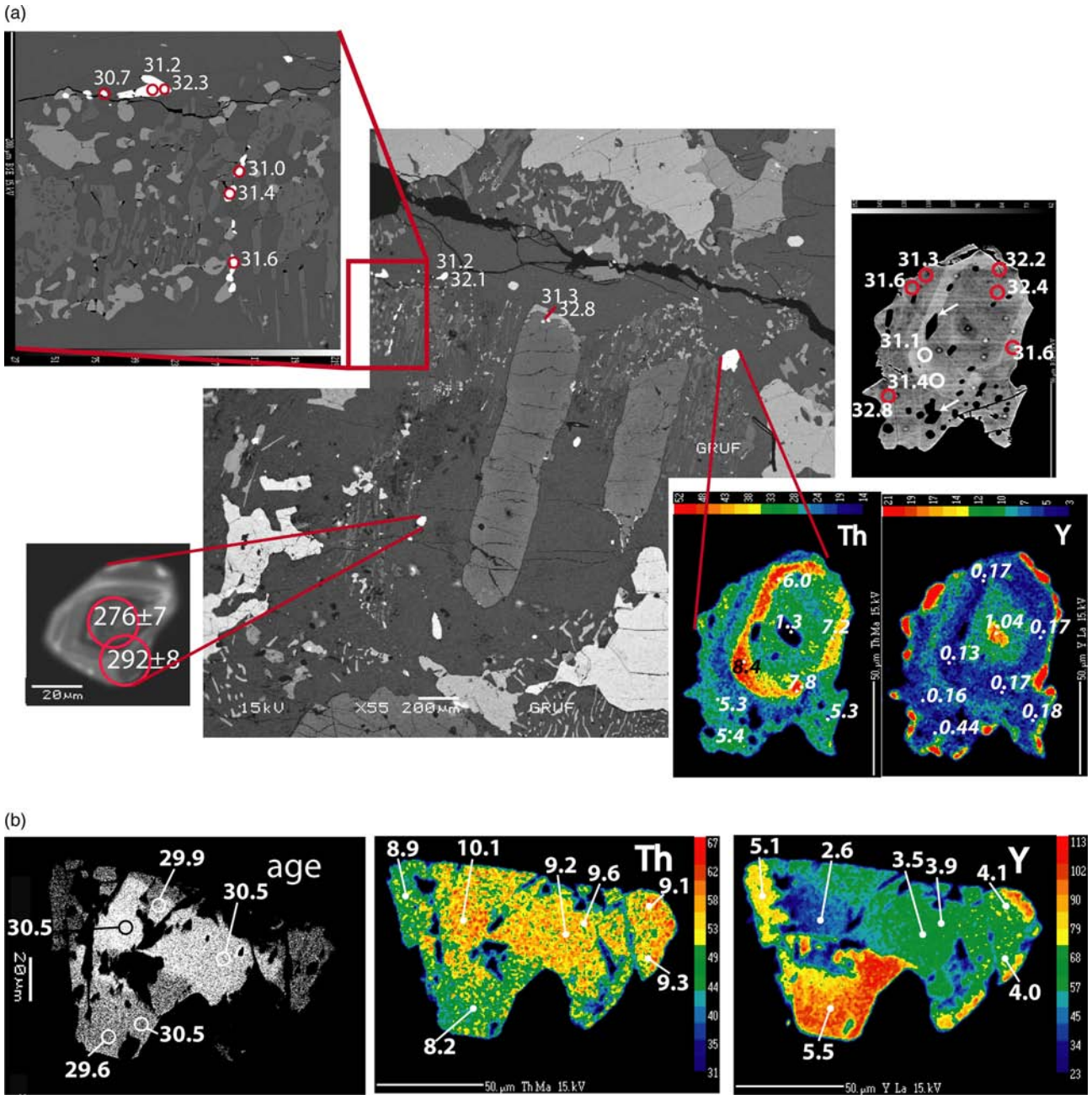


**Fig. 6.** (**a**) BSE images of Figure 2b and of the monazites in Spr, Crd and in clusters in late symplectites; cathodoluminescence of a zircon in Crd. $ThO_2$ and $Y_2O_3$ X-ray maps (spots; in wt%) in the crystal T50M1 and $^{208}Pb/^{232}Th$ ages (circles) in Ma (with ±1.1 Ma for the monazites). Black inclusions are needles of sillimanite; arrows: diamond-shaped basal sections. (**b**) $ThO_2$ and $Y_2O_3$ X-ray maps (spots; in wt%) and BSE image and $^{208}Pb/^{232}Th$ ages (circles) in Ma with ±1.1Ma for a monazite in the charnockite portion of the rock (crystal T12M1).

lithologies is improbable, as also suggested by McDade & Harley (2001), unless a large amount of fluid is added. It is very unlikely that this fluid-assisted migmatization event in amphibolite-facies conditions could be responsible for all the textures observed in the UHT granulites. There is no evidence in the retrograde reactions of significant fluid input, as argued by Galli *et al.* (2011). In contrast, we propose that all the metamorphic textures in the Mg–Al granulites correspond with the UHT conditions during Alpine time, as demonstrated by the age recorded in the monazites equilibrated with the UHT mineral assemblages.

### *A model for the evolution of the Gruf granulites and charnockites*

Based on the petrological observations and geochronological results obtained in our sample we propose the following model for the evolution of the Gruf granulites and charnockites through time. The oldest ages obtained in the zircons from our UHT granulite sample are between 304 ± 12 Ma and 247 ± 6 Ma. These ages, despite being slightly older, are similar to those measured by Galli *et al.* (2012) and Liati & Gebauer (2003) in the Gruf UHT granulites. Older ages at 513 ± 8 Ma and 453 ± 8 Ma (weighted average ages in magmatic zircon cores) have only been reported in an enclave-rich biotite orthogneiss in the Gruf complex (Galli *et al.* 2012). Our results suggest that oscillatory zoned zircons from the UHT granulites crystallized in Permian–Triassic times during a partial melting event. This Paleozoic anatectic event occurred under granulite-facies conditions, as shown by the presence of the charnockitic paragenesis included in the zircon cores (Galli *et al.* 2013), inducing the formation of both charnockitic melt and restitic/resister rocks, the precursor of the sapphirine-bearing granulites. Unfortunately, the few tiny inclusions observed in the zircon grains

**Table 1.** *Electron microprobe analyses of the monazites*

| | G | G | | G | G | | | Ch | | | G | | Ch | | G | | G | G | G | G |
|---|---|---|---|---|---|---|---|---|---|---|---|---|---|---|---|---|---|---|---|---|
| Analyses | 2 | 7 | 14 | 17 | 18 | 23 | 25 | 32 | 33 | 34 | 42 | 45 | 49 | 53 | 56 | 57 | 58 | 59 | 61 | 64 |
| | T50-M2 | T50-M1 | | i sapphirine | T50-cluster | | | T14 M1 | | | T13 M1 | | T12-M1 | | T10bis-M2 | | T10 bis | T10bisM1 | T18-i OPX | T33-i OPX |
| $SiO_2$ | 0.17 | 0.27 | 0.12 | 0.19 | 0.21 | 0.10 | 0.16 | 0.25 | 0.31 | 0.47 | 0.22 | 0.38 | 0.39 | 0.59 | 0.41 | 0.32 | 0.19 | 1.34 | 0.19 | 0.32 |
| $P_2O_5$ | 30.15 | 29.51 | 29.77 | 29.54 | 29.93 | 29.99 | 29.67 | 30.20 | 29.96 | 29.65 | 30.29 | 29.57 | 30.02 | 29.09 | 29.60 | 29.57 | 29.80 | 27.70 | 29.65 | 30.12 |
| $Ce_2O_3$ | 29.92 | 28.92 | 30.59 | 29.74 | 29.23 | 30.28 | 29.79 | 25.18 | 25.44 | 25.61 | 28.36 | 25.20 | 24.73 | 25.71 | 29.57 | 29.48 | 29.22 | 30.89 | 29.94 | 27.14 |
| $La_2O_3$ | 13.58 | 13.48 | 14.31 | 13.26 | 13.14 | 13.30 | 13.59 | 10.70 | 11.09 | 11.10 | 12.51 | 11.39 | 10.70 | 11.22 | 13.47 | 13.39 | 13.20 | 14.78 | 13.59 | 12.29 |
| $Pr_2O_3$ | 3.30 | 3.18 | 3.10 | 3.39 | 3.19 | 3.45 | 3.21 | 2.78 | 2.98 | 2.87 | 2.93 | 3.01 | 2.77 | 2.89 | 3.08 | 3.09 | 3.23 | 3.65 | 3.05 | 3.02 |
| $Nd_2O_3$ | 11.49 | 10.97 | 11.95 | 11.58 | 11.36 | 11.32 | 11.06 | 9.88 | 10.44 | 10.49 | 10.75 | 8.71 | 10.32 | 11.27 | 11.65 | 11.66 | 10.92 | 11.99 | 10.52 | 11.02 |
| $Sm_2O_3$ | 1.95 | 1.46 | 1.54 | 1.66 | 1.74 | 2.17 | 1.66 | 2.14 | 1.90 | 2.03 | 1.92 | 1.64 | 1.85 | 1.82 | 1.73 | 1.52 | 1.75 | 1.19 | 1.77 | 1.74 |
| $Gd_2O_3$ | 1.33 | 0.44 | 0.69 | 1.09 | 1.54 | 1.58 | 1.06 | 2.44 | 1.91 | 2.05 | 1.39 | 1.01 | 2.04 | 1.60 | 1.07 | 1.11 | 1.01 | 0.64 | 0.91 | 1.82 |
| $Y_2O_3$ | 0.39 | 0.13 | 0.35 | 0.31 | 0.50 | 0.69 | 0.32 | 4.78 | 3.78 | 3.24 | 0.98 | 0.47 | 3.89 | 2.63 | 0.27 | 0.58 | 0.91 | 0.14 | 0.65 | 2.14 |
| CaO | 1.34 | 1.75 | 1.16 | 1.39 | 1.45 | 1.15 | 1.46 | 1.61 | 1.76 | 1.77 | 1.83 | 2.90 | 1.78 | 1.67 | 1.31 | 1.45 | 1.53 | 0.44 | 1.53 | 1.49 |
| $ThO_2$ | 5.79 | 8.43 | 5.15 | 6.42 | 6.07 | 3.92 | 6.73 | 7.84 | 8.75 | 9.32 | 6.78 | 10.82 | 9.59 | 10.07 | 7.17 | 5.74 | 5.19 | 6.96 | 5.48 | 8.00 |
| $UO_2$ | 0.98 | 0.33 | 0.50 | 0.78 | 0.83 | 1.35 | 0.75 | 0.74 | 0.41 | 0.32 | 2.05 | 3.50 | 0.40 | 0.26 | 0.45 | 1.29 | 2.01 | 0.20 | 1.78 | 0.37 |
| PbO | 0.03 | 0.00 | 0.00 | 0.04 | 0.01 | 0.00 | 0.00 | 0.00 | 0.03 | 0.00 | 0.01 | 0.02 | 0.00 | 0.01 | 0.00 | 0.00 | 0.01 | 0.00 | 0.03 | 0.01 |
| Total | 100.41 | 98.87 | 99.23 | 99.38 | 99.20 | 99.30 | 99.48 | 98.54 | 98.76 | 98.93 | 100.00 | 98.63 | 98.49 | 98.83 | 99.76 | 99.21 | 98.96 | 99.90 | 99.08 | 99.47 |
| Si | 0.007 | 0.011 | 0.005 | 0.007 | 0.008 | 0.004 | 0.007 | 0.010 | 0.012 | 0.018 | 0.009 | 0.015 | 0.015 | 0.023 | 0.016 | 0.013 | 0.007 | 0.054 | 0.008 | 0.012 |
| P | 0.996 | 0.991 | 0.995 | 0.990 | 0.997 | 0.999 | 0.992 | 0.995 | 0.991 | 0.984 | 0.998 | 0.990 | 0.993 | 0.975 | 0.987 | 0.988 | 0.995 | 0.941 | 0.992 | 0.995 |
| Ce | 0.427 | 0.420 | 0.442 | 0.431 | 0.421 | 0.436 | 0.431 | 0.359 | 0.364 | 0.368 | 0.404 | 0.365 | 0.354 | 0.373 | 0.426 | 0.426 | 0.422 | 0.454 | 0.433 | 0.388 |
| La | 0.195 | 0.197 | 0.208 | 0.194 | 0.191 | 0.193 | 0.198 | 0.154 | 0.160 | 0.161 | 0.179 | 0.166 | 0.154 | 0.164 | 0.196 | 0.195 | 0.192 | 0.219 | 0.198 | 0.177 |
| Pr | 0.047 | 0.046 | 0.045 | 0.049 | 0.046 | 0.049 | 0.046 | 0.039 | 0.042 | 0.041 | 0.042 | 0.043 | 0.039 | 0.042 | 0.044 | 0.044 | 0.046 | 0.053 | 0.044 | 0.043 |
| Nd | 0.160 | 0.155 | 0.169 | 0.164 | 0.160 | 0.159 | 0.156 | 0.137 | 0.146 | 0.147 | 0.149 | 0.123 | 0.144 | 0.159 | 0.164 | 0.164 | 0.154 | 0.172 | 0.149 | 0.153 |
| Sm | 0.026 | 0.020 | 0.021 | 0.023 | 0.024 | 0.029 | 0.023 | 0.029 | 0.026 | 0.027 | 0.026 | 0.022 | 0.025 | 0.025 | 0.023 | 0.021 | 0.024 | 0.016 | 0.024 | 0.023 |
| Eu | 0.000 | 0.000 | 0.000 | 0.000 | 0.000 | 0.000 | 0.000 | 0.000 | 0.000 | 0.000 | 0.000 | 0.000 | 0.000 | 0.000 | 0.000 | 0.000 | 0.000 | 0.000 | 0.000 | 0.000 |
| Gd | 0.017 | 0.006 | 0.009 | 0.014 | 0.020 | 0.021 | 0.014 | 0.031 | 0.025 | 0.027 | 0.018 | 0.013 | 0.026 | 0.021 | 0.014 | 0.015 | 0.013 | 0.009 | 0.012 | 0.023 |
| Y | 0.008 | 0.003 | 0.007 | 0.006 | 0.010 | 0.015 | 0.007 | 0.099 | 0.079 | 0.068 | 0.020 | 0.010 | 0.081 | 0.055 | 0.006 | 0.012 | 0.019 | 0.003 | 0.014 | 0.044 |
| Ca | 0.056 | 0.074 | 0.049 | 0.059 | 0.061 | 0.048 | 0.062 | 0.067 | 0.074 | 0.075 | 0.076 | 0.123 | 0.074 | 0.071 | 0.055 | 0.062 | 0.064 | 0.019 | 0.065 | 0.062 |
| Th | 0.051 | 0.076 | 0.046 | 0.058 | 0.054 | 0.035 | 0.060 | 0.069 | 0.078 | 0.083 | 0.060 | 0.097 | 0.085 | 0.091 | 0.064 | 0.052 | 0.047 | 0.064 | 0.049 | 0.071 |
| U | 0.008 | 0.003 | 0.004 | 0.007 | 0.007 | 0.012 | 0.007 | 0.006 | 0.004 | 0.003 | 0.018 | 0.031 | 0.004 | 0.002 | 0.004 | 0.011 | 0.018 | 0.002 | 0.016 | 0.003 |
| Pb | 0.000 | 0.000 | 0.000 | 0.000 | 0.000 | 0.000 | 0.000 | 0.000 | 0.000 | 0.000 | 0.000 | 0.000 | 0.000 | 0.000 | 0.000 | 0.000 | 0.000 | 0.000 | 0.000 | 0.000 |
| Total | 2.000 | 2.001 | 2.001 | 2.002 | 1.999 | 2.000 | 2.001 | 1.997 | 1.999 | 2.001 | 1.998 | 2.000 | 1.995 | 2.001 | 1.999 | 2.003 | 2.001 | 2.006 | 2.003 | 1.995 |

G, granulite domain; Ch, charnockite domain.

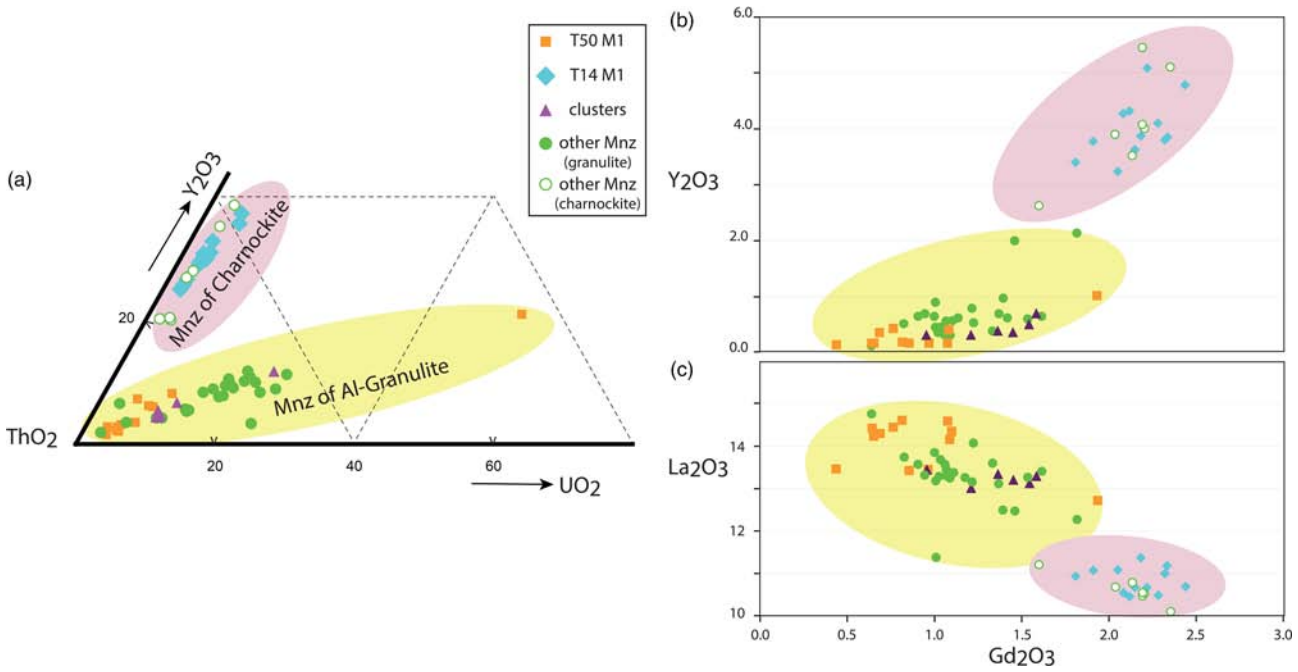


**Fig. 7.** Chemical composition of the monazites: (**a**) ternary diagram showing the relative $Y_2O_3$, $ThO_2$ and $UO_2$ (wt%) contents; (**b**) $Y_2O_3$ versus $Gd_2O_3$; (**c**) $La_2O_3$ versus $Gd_2O_3$.

do not allow precise determination of what the mineral assemblage was in this precursor during the Paleozoic event. We suggest that the precursor of the sapphirine-bearing granulites was a biotite–cordierite-rich selvedge probably also containing orthopyroxene, and garnet could have been added. Considering the abundance of the monazites in our sample, it is likely that monazites were present during Permian times. In Alpine times, UHT metamorphism occurred during a short-lived event (less than 5 Ma) between 30 and 34 Ma recorded by both zircon rims and monazites. UHT metamorphic conditions at 920–940°C/0.85–0.95 GPa (Galli *et al.* 2011) are responsible for the complete re-crystallization of both the charnockites and the Bt–Cd–Grt(?)–Opx(?)-bearing rocks and enabled the development of the UHT paragenesis appearance: Al-rich Opx–Sil–Spr–Bt–Grt–Crd–Rt–Ap–Zrn–Mnz in the Mg–Al granulite and Opx, Bt, Kfs, ± Pl, Qz, Zrn, Mnz and Ap in the charnockite. In both the charnockites and the Mg–Al granulites, this UHT event is responsible for the partial dissolution of the Paleozoic zircons and the growth of the Alpine rims. Because no Paleozoic ages were found in monazites from our samples (as well as in the previous monazite study, Schmitz *et al.* 2009), crystallization processes for the Alpine monazites are more difficult to assess. Two processes can be proposed: crystallization from a mineral precursor, such as allanite or apatite, or complete recrystallization of an earlier monazite generation, possibly late Carboniferous–Permian in age. In our sample petrographic evidence of a monazite precursor is missing and it is not possible to solve the question in the present context.

### *Geodynamic implications and the origin of UHT metamorphism in the central Alps*

The oldest ages we obtained in the zircon cores of between 304 ± 12 Ma and 247 ± 6 Ma, interpreted as the age of charnockitization, unknown elsewhere in the Penninic domain of the Central Alps (Galli *et al.* 2011), developed during the Permian–Triassic high thermal regime responsible for HT–LP metamorphism widespread in the Austroalpine and Southalpine domains (Lardeaux & Spalla 1991; Diella *et al.* 1992; Bertotti *et al.* 1993; Barboza & Bergantz 2000; Müntener *et al.* 2000; Galli *et al.* 2013; Marotta *et al.* 2018). These granulites are interpreted as residual and refractory rocks following partial melting events and extensive melt loss. This process is responsible for the differentiation of the continental crust via fluid-absent melting reactions involving muscovite and biotite (and amphibole in metabasic rocks) destabilization. As a consequence, the precursor of the Al–Mg granulites of the Gruf complex acquired its restitic character during this post-Hercynian event.

UHT metamorphism occurs at temperatures above the fluid-absent melting in most crustal rocks which is an endothermic process that consumes heat and buffers the temperature (Vielzeuf & Holloway 1988; Stüwe 1995). Thus partial melting limits heat production, avoiding a fertile crust to attain UHT. Nevertheless, UHT conditions are more easily reached in refractory/restitic rocks and develop preferentially in terrains that previously underwent metamorphism and melt loss (Clark *et al.* 2011; Kelsey & Hand 2015). The Gruf complex is the sole unit in the Penninic Domain of the Central Alps recording Permian–Triassic granulitic metamorphism, which permitted its rocks to reach and record UHT conditions during the Alpine cycle.

Zircon and monazite ages, together with their microstructural relationships with granulite-facies minerals, show that the typical UHT paragenesis crystallized in Alpine times during a short-lived event (less than 5 Ma) between 34 and 30 Ma. These results are in agreement with garnet diffusion modelling proposed by Galli *et al.* (2011), also suggesting that UHT metamorphism was brief. This UHT metamorphism was contemporaneous with the Bergell tonalite–granodiorite intrusion dated between 33 and 28 Ma (Berger *et al.* 1996) and the beginning of the anatectic event in the southern part of the Central Alps at 32 Ma (Köppel *et al.* 1981; Berger *et al.* 2009; Rubatto *et al.* 2009). Secondary symplectites in the Mg–Al granulites just following the UHT peak conditions were equilibrated in the same conditions as the Lepontine migmatization (e.g. Engi *et al.* 1995; Burri *et al.* 2005). However, the 38–34 Ma UHP metamorphism in the Lepontine domain was quickly followed by a fast exhumation, then the UHT event and the final amphibolite-facies migmatization (Brouwer *et al.* 2004). This fast exhumation is related to a short-lived (less than 4 Ma) episode of lithospheric thinning associated with a rise of hot asthenospheric material (Brouwer *et al.* 2004) from 34 Ma to 32–30 Ma (Beltrando *et al.* 2010). Oalmann *et al.* (2016) proposed that similar lithospheric

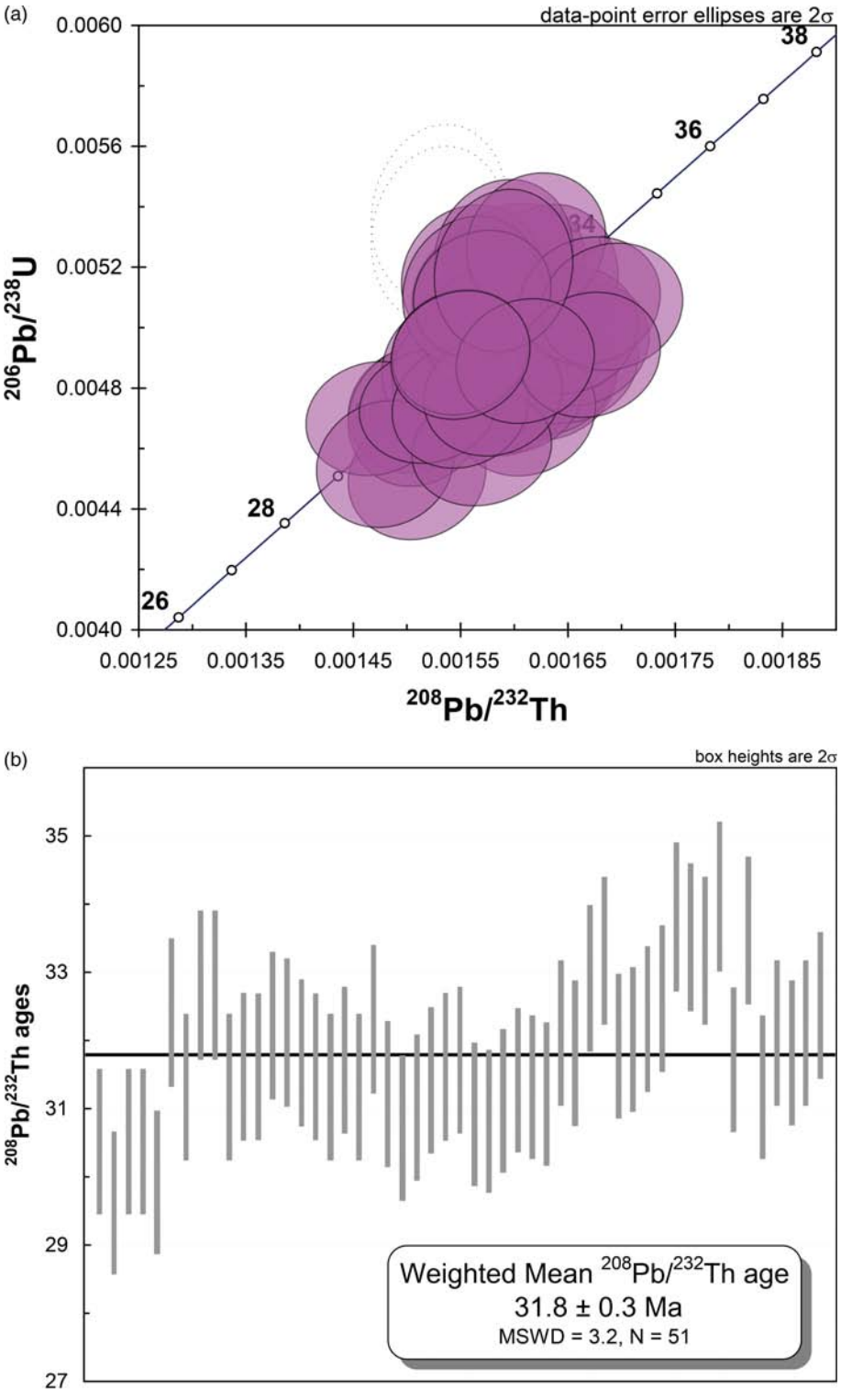


**Fig. 8.** Geochronological results: (**a**) $^{208}Pb/^{232}Th$ versus $^{206}Pb/^{238}U$ diagram for the monazite; (**b**) weighted average $^{208}Pb/^{232}Th$ ages in monazite;

thinning associated with slab breakoff or rollback and asthenospheric upwelling could also be responsible for the short-lived Alpine UHT metamorphism in the Gruf complex. A similar geodynamic context is proposed for another example of Phanerozoic UHT metamorphism (16 Ma) of the island of Seram (Indonesia), where the UHT conditions were produced by slab rollback-driven lithospheric extension and the exhumation of hot subcontinental lithospheric mantle (Pownall *et al.* 2014; Pownall 2015). Harley (2016) proposed that a shorter duration UHT granulite event can be formed as a consequence of severe lithospheric thinning and crustal extension accompanied by voluminous magmatism in arc settings affected by subduction rollback. Brouwer *et al.* (2004) noticed that heating by slab detachment is fast and transient (more than 100°C in up to 10 Ma), whereas radiogenic heating requires time spans of the order of tens of millions of years and cessation of the subduction process. Finally, Perchuk *et al.* (in press) used numerical models to explain ultra-hot orogeny and showed that UHT conditions at the bottom of the crust might be produced by lateral propagation of the hot asthenospheric front during plate convergence associated with lithospheric delamination. In this model, a close relationship between HT–UHT metamorphism and tonalitic magmatism is proposed. This could explain the relationship between the Gruf UHT metamorphism and the Bergell intrusion, which is one of the main Periadriatic igneous bodies emplaced during Late Alpine times, characterized by

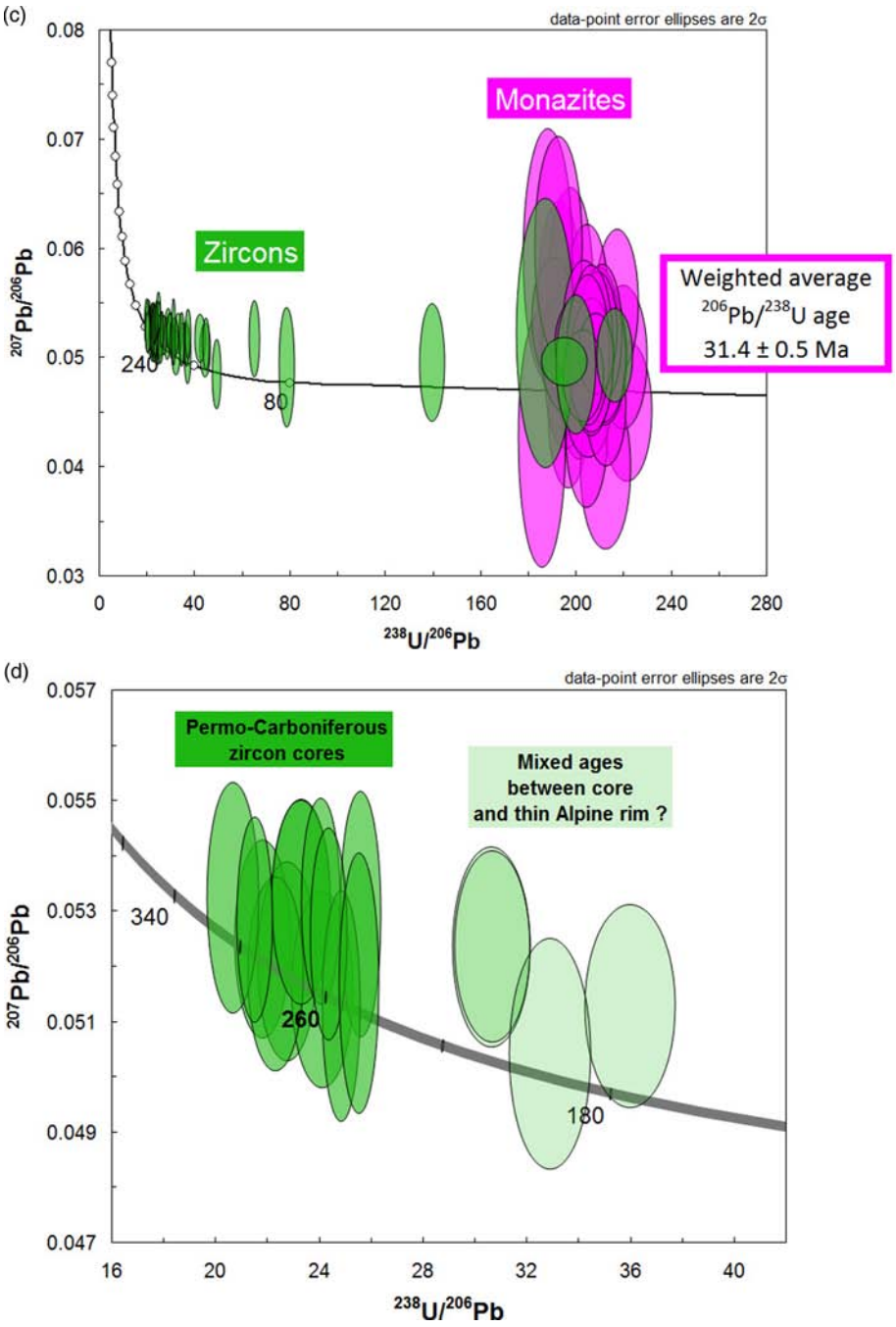


**Fig. 8.** *Continued.* (**c**) Tera–Wasserburg diagram showing the zircon and monazite data (for more clarity, only concordant U/Pb data are shown); (**d**) Tera–Wasserburg diagram showing U/Pb results for zircon cores with U content ≤1000 ppm and zircon grain without apparent Alpine rim in CLI.

an enriched mantle source (von Blanckenburg *et al.* 1998) and interpreted as triggered by post-collisional slab breakoff.

## Conclusions

*In situ* and in context zircon dating on zircon from a restitic granulite within charnockites give both Permian–Triassic (304–247 Ma) and Alpine ages (*c.* 34–30 Ma). $^{208}Pb/^{232}Th$ ages measured in monazite from the same sample yield a weighted average age of 31.8 ± 0.3 Ma (MSWD = 3.2, $n = 51$) interpreted as the time of complete (re-) crystallization of the monazite in equilibrium with the UHT paragenesis. The Alpine UHT event was thus recorded by zircon rims and monazites. The oldest ages we obtained in the zircons, between 304 ± 12 and 247 ± 6 Ma, are interpreted as the age of the charnockitization during which the precursor of the Al–Mg granulites of the Gruf complex acquired its restitic character. Our results show that the Gruf complex is the sole Penninic unit in the Central Alps recording post-Hercynian granulitic metamorphism, which means that it attains and records UHT conditions during the Alpine cycle. The typical UHT paragenesis crystallized in Alpine times during a short-lived event (less than 5 Ma) related to lithospheric thinning associated with a rise of hot asthenospheric material.

**Acknowledgements** The subject editor Igor Villa and the two reviewers Simon Harley and Jean-Marc Lardeaux are thanked for their constructive comments. We also thank Dr E. Bruand for reading the English. Thanks are due to Jean Luc Devidal and Jean-Marc Hénot for their help in the use of EMP and SEM.

**Funding** This research was financed by the French Government Laboratory of Excellence initiative n° ANR-10-LABX-0006. This is Laboratory of Excellence ClerVolc contribution number 306.

*Scientific editing by Igor Maria Villa*

## References

Barboza, S.A. & Bergantz, G.W. 2000. Metamorphism and anatexis in the mafic complex contact aureole, Ivrea Zone, northern Italy. *Journal of Petrology*, **41**, 1307–1327, https://doi.org/10.1093/petrology/41.8.1307

Barker, F. 1964. Sapphirine-bearing rock, Val Codera, Italy. *American Mineralogist*, **49**, 146–152.

Beltrando, M., Lister, G.S., Rosenbaum, G., Richards, S. & Forster, M.A. 2010. Recognizing episodic lithospheric thinning along a convergent plate margin: The example of the Early Oligocene Alps. *Earth-Science Reviews*, **103**, 81–98, https://doi.org/10.1016/j.earscirev.2010.09.001

Berger, A., Rosenberg, C. & Schmid, S.M. 1996. Ascent, emplacement and exhumation of the Bergell pluton within the Southern Steep Belt of the Central Alps. *Schweizerische Mineralogische und Petrographische Mitteilungen*, **76**, 357–382.

Berger, A., Rosenberg, C. & Schaltegger, U. 2009. Stability and isotopic dating of monazite and allanite in partially molten rocks: examples from the Central Alps. *Swiss Journal of Geoscience*, **102**, 15–29, https://doi.org/10.1007/s00015-009-1310-8

Bertotti, G., Siletto, G.B. & Spalla, M.I. 1993. Deformation and metamorphism associated with crustal rifting: Permian to Liassic evolution of the Lake Lugano-Lake Como area (Southern Alps). *Tectonophysics*, **226**, 271–284, https://doi.org/10.1016/0040-1951(93)90122-Z

Brodie, K.H., Rex, D. & Rutter, E.H. 1989. On the age of deep crustal extensional faulting in the Ivrea zone, Northern Italy. *In*: Coward, M. P., Dietrich, D. & Park, R. G. (eds) *Alpine Tectonics*. Geological Society, London, Special Publications, **45**, 203–210, https://doi.org/10.1144/GSL.SP.1989.045.01.11

Brouwer, F.M., van de Zedde, D.M., Wortel, M.J. & Vissers, R.L. 2004. Late-orogenic heating during exhumation: Alpine PTt trajectories and thermo-mechanical models. *Earth and Planetary Science Letters*, **220**, 185–199, https://doi.org/10.1016/S0012-821X(04)00050-0

Brown, M. 2007. Metamorphic conditions in orogenic belts: a record of secular change. *International Geological Review*, **49**, 193–234, https://doi.org/10.2747/0020-6814.49.3.193

Brown, M. 2008. Granites, migmatites and residual granulites: relationships and processes. *In:* Sawyer, E.W. & Brown, M. (eds) *Working With Migmatites*. Mineralogical Association of Canada Short Course, **38**, 97–144.

Burri, T., Berger, A. & Engi, M. 2005. Tertiary migmatites in the Central Alps: regional distribution, field relations, conditions of formation, and tectonic implications. *Schweizerische Mineralogische und Petrographische Mitteilungen*, **85**, 215–232.

Cherniak, D.J., Watson, B.E., Grove, M. & Harrison, T.M. 2004. Pb diffusion in monazite: a combined RBS/SIMS study. *Geochimica et Cosmochimica Acta*, **68**, 829–840, https://doi.org/10.1016/j.gca.2003.07.012

Clark, C., Fitzsimons, I.C.W., Healy, D. & Harley, S.L. 2011. - How does the continental crust get really hot? *Elements*, **7**, 235–240, https://doi.org/10.2113/gselements.7.4.235

Cornelius, H.P. 1916. Ein alpines Vorkommen von Sapphirine. *Centralblatt für Mineralogie, Geologie und Paläontologie,* Jahrgang 1916, 265–269.

Cornelius, H.P. & Dittler, E. 1929. Zur Kenntnis des Sapphirinvorkommens von Alpe Bresciadega in Val Codera (Italien, Prov. Sondrio). *Neues Jahrbuch Fur Mineralogie-Abhandlungen*, **59**, 27–64.

Davies, J.H. & Von Blanckenburg, F. 1995. Slab breakoff: A model of lithosphere detachment and its test in the magmatism and deformation of collisional orogens. *Earth and Planetary Science Letters*, **129**, 85–102, https://doi.org/10.1016/0012-821X(94)00237-S

Didier, A., Bosse, V., Cherneva, Z., Gautier, P., Georgieva, M., Paquette, J.L. & Gerdjikov, I. 2014. Syn-deformation fluid-assisted growth of monazite during renewed high-grade metamorphism in metapelites of the Central Rhodope (Bulgaria, Greece). *Chemical Geology*, **381**, 206–222, https://doi.org/10.1016/j.chemgeo.2014.05.020

Didier, A., Bosse, V. *et al.* 2015. NanoSIMS mapping and LA-ICP-MS chemical and U–Th–Pb data in monazite from a xenolith enclosed in andesite (Central Slovakia Volcanic Field). *Contributions to Mineralogy & Petrology*, **170**, 45, https://doi.org/10.1007/s00410-015-1200-1

Diella, V., Spalla, M.I. & Tunesi, A. 1992. Contrasted thermo-mechanical evolutions in the Southalpine metamorphic basement of the Orobic Alps (Central Alps, Italy). *Journal of Metamorphic Geology*, **10**, 203–219, https://doi.org/10.1111/j.1525-1314.1992.tb00079.x

Droop, G.T.R. & Bucher-Nurminen, K. 1984. Reaction textures and metamorphic evolution of sapphirine-bearing granulites from the Gruf Complex, Italian Central Alps. *Journal of Petrology*, **25**, 766–803.

Engi, M., Todd, C.S. & Schmatz, D.R. 1995. Tertiary metamorphic conditions in the eastern Lepontine Alps. *Schweizerische Mineralogische und Petrographische Mitteilungen*, **75**, 347–369.

Engi, M., Berger, A. & Roselle, G.T. 2001. Role of the tectonic accretion channel in collisional orogeny. *Geology*, **29**, 1143–1146.

Engi, M., Bousquet, R. & Berger, A. 2004. Explanatory notes to the map: Metamorphic structure of the Alps – Central Alps. *Mitteilungen der Österreichischen Mineralogischen Gesellschaft*, **149**, 157–173.

Galli, A., Le Bayon, B., Schmidt, M.W., Burg, J.P., Caddick, M.J. & Reusser, E. 2011. Granulites and charnockites of the Gruf Complex: evidence for Permian ultra-high temperature metamorphism in the Central Alps. *Lithos*, **124**, 17–45, https://doi.org/10.1016/j.lithos.2010.08.003

Galli, A., Le Bayon, B., Schmidt, M.W., Burg, J.P., Reusser, E., Sergeev, S.A. & Larionov, A. 2012. U–Pb zircon dating of the Gruf Complex: disclosing the late Variscan granulitic lower crust of Europe stranded in the Central Alps. *Contributions to Mineralogy and Petrology*, **163**, 353–378, https://doi.org/10.1007/s00410-011-0676-6

Galli, A., Le Bayon, B., Schmidt, M.W., Burg, J.P. & Reusser, E. 2013. Tectonometamorphic history of the Gruf complex (Central Alps): exhumation of a granulite–migmatite complex with the Bergell pluton. *Swiss Journal of Geoscience*, **106**, 33–62, https://doi.org/10.1007/s00015-013-0120-1

Guevara, V.E. & Caddick, M.J. 2016. Shooting at a moving target: phase equilibria modelling of high temperature metamorphism. *Journal of Metamorphic Geology*, **34**, 209–235, https://doi.org/10.1111/jmg.12179

Harley, S.L. 1998. On the occurrence and characterization of ultrahight-emperature crustal metamorphism. *In:* Treloar, P.J. & O'Brien, P.J. (eds) *What Drives Metamorphism and Metamorphic Relations?* Geological Society, London, Special Publications, **138**, 81–107, https://doi.org/10.1144/GSL.SP.1996.138.01.06

Harley, S.L. 2016. A matter of time: the importance of the duration of UHT metamorphism. *Journal of Mineralogical and Petrological Sciences*, **111**, 50–72, https://doi.org/10.2465/jmps.160128

Kelly, N.M., Harley, S.L. & Möller, A. 2012. Complexity in the behavior and recrystallization of monazite during high-T metamorphism and fluid infiltration. *Chemical Geology*, **322–323**, 192–208, https://doi.org/10.1016/j.chemgeo.2012.07.00

Kelsey, D.E. & Hand, M. 2015. On ultrahigh temperature crustal metamorphism: Phase equilibria, trace element thermometry, bulk composition, heat sources, timescales and tectonic settings. *Geoscience Frontiers*, **6**, 311–356, https://doi.org/10.1016/j.gsf.2014.09.006

Kelsey, D.E., White, R.W. & Powell, R. 2003. Orthopyroxene–sillimanite–quartz assemblages: distribution, petrology, quantitative P–T–X constraints and P–T paths. *Journal of Metamorphic Geology*, **21**, 439–453, https://doi.org/10.1046/j.1525-1314.2003.00456.x

Köppel, V., Günthert, A. & Grünenfelder, M. 1981. Patterns of U–Pb zircon and monazite ages in polymetamorphic units of the Swiss Alps. *Schweizerische Mineralogische und Petrographische Mitteilungen*, **61**, 97–119.

Korhonen, F.J., Clark, C., Brown, M., Bhattacharya, S. & Taylor, R. 2013. How long-lived is ultrahigh temperature (UHT) metamorphism? Constraints from zircon and monazite geochronology in the Eastern Ghats orogenic belt, India. *Precambrian Research*, **234**, 322–350, https://doi.org/10.1016/j.precamres.2012.12.001

Lardeaux, J.M. & Spalla, I. 1991. From granulites to eclogites in the Sesia zone (Italian Western Alps): a record of opening and closure of the Piedmont ocean. *Journal of Metamorphic Geology*, **9**, 35–59.

Liati, A. & Gebauer, D. 2003. Geochronological constraints for the time of metamorphism in the Gruf Complex (Central Alps) and implications for the Adula-Cima Lunga nappe system. *Schweizerische Mineralogische und Petrographische Mitteilungen*, **83**, 159–172.

Manzotti, P. & Zucali, M. 2013. The pre-Alpine tectonic history of the Austroalpine continental basement in the Valpelline unit (Western Italian Alps). *Geological Magazine*, **150**, 153–172, https://doi.org/10.1017/S0016756812000441

Manzotti, P., Rubatto, D., Darling, J., Zucali, M., Cenki-Tok, B. & Engi, M. 2012. From Permo-Triassic lithospheric thinning to Jurassic rifting at the Adriatic margin: Petrological and geochronological record in Valtournenche (Western Italian Alps). *Lithos*, **146–147**, 276–292, https://doi.org/10.1016/j.lithos.2012.05.007

Marotta, A.M., Gosso, G. & Spalla, M.I. 2009. Upper and lower crustal evolution during lithospheric extension: Numerical modelling and natural footprints from the European Alps. *In*: Ring, U. & Wernicke, B. (eds) *Extending a Continent: Architecture, Rheology and Heat Budget*. Geological Society, London, Special Publications, **321**, 33–72, https://doi.org/10.1144/SP321.3

Marotta, A.M., Roda, M., Conte K. & Spalla, M.I. 2018. Thermo-mechanical numerical model of the transition from continental rifting to oceanic spreading: the case study of the Alpine Tethys. *Geological Magazine*, **155**, 250–279, https://doi.org/10.1017/S0016756816000856

McDade, P. & Harley, S.L. 2001. A petrogenetic grid for aluminous granulite facies metapelites in the KFMASH system. *Journal of Metamorphic Geology*, **19**, 45–59, https://doi.org/10.1046/j.0263-4929.2000.00296.x

McLellan, E.L. 1989. Sequential formation of subsolidus and anatectic migmatites: response to thermal evolution, eastern Scotland. *Journal of Geology*, **97**, 165–182.

Montel, J.M. 1986. Experimental determination of the solubility of Ce-monazite in $SiO_2$–$Al_2O_3$–$K_2O$–$Na_2O$ melts at 800°C, 2 kbar, under $H_2O$-saturated conditions. *Geology*, **14**, 659–662.

Montel, J.M., Didier, J. & Pichavant, M. 1991. Origin of surmicaceous enclaves in intrusive granites. *In*: *Developments in Petrology : Enclaves and Granite Petrology*. Elsevier, 509–528.

Müntener, O., Hermann, J. & Trommsdorff, V. 2000. Cooling history and exhumation of lower crustal granulite and upper Mantle (Malenco, eastern Central Alps). *Journal of Petrology*, **41**, 175–200.

Niggli, E. 1974. Metamorphism and tectonics of the Alps. *Memorie della Società geologica Italiana*, **13**, 285–289.

Oalmann, J., Möller, A. & Bousquet, R. 2013. P–T modelling reveals juxtaposition of units within the Gruf Complex (Central Alps) during orogenesis. *Mineralogical Magazine*, **77**, 1873, https://doi.org/10.1180/minmag.2013.077.5.15

Oalmann, J., Möller, A. & Bousquet, R. 2016. Unravelling the P–T–t evolution of the crust of the Gruf complex by in situ accessory mineral dating and

thermometry combined with P–T modelling of microdomains. Paper presented at the European Mineralogical Conference, Rimini.

Paquette, J.-L. & Tiepolo, M. 2007. High resolution (5 μm) U–Th–Pb isotopes dating of monazite with excimer laser ablation (ELA)-ICPMS. *Chemical Geology*, **240**, 222–237, https://doi.org/10.1016/j.chemgeo.2007.02.014

Paquette, J.L., Goncalves, P., Devouard, B. & Nicollet, C. 2004. Micro-drilling ID-TIMS U–Pb dating of single monazites: A new method to unravel complex poly-metamorphic evolutions. Application to the UHT granulites of Andriamena (North-Central Madagascar). *Contributions to Mineralogy and Petrology*, **147**, 110–122, https://doi.org/10.1007/s00410-003-0549-8

Paquette, J.L., Piro, J.L., Devidal, J.L., Bosse, V. & Didier, A. 2014. Sensitivity enhancement in LA-ICP-MS by N2 addition to carrier gas: application to radiometric dating of U–Th bearing minerals. *Agilent ICP-MS Journal*, **58**, 4–5.

Perchuk, A.L., Safonov, O.G., Smit, C.A, van Reenen, D.D, Zakharov, V.S. & Gerya, T.V. In press. Precambrian ultra-hot orogenic factory: Making and reworking of continental crust. *Tectonophysics*, corrected proof online December 7, 2016, https://doi.org/10.1016/j.tecto.2016.11.041

Peressini, G., Quick, J.E., Sinigoi, S., Hofmann, A.W. & Fanning, M. 2007. Duration of a large mafic intrusion and heat transfer in the lower crust: a SHRIMPU–Pb zircon study in the Ivrea-Verbano Zone (Western Alps, Italy). *Journal of Petrology*, **48**, 1185–1218, https://doi.org/10.1093/petrology/egm014

Pownall, J.M. 2015. UHT metamorphism on Seram, eastern Indonesia: reaction microstructures and P–T evolution of spinel-bearing garnet–sillimanite granulites from the Kobipoto Complex. *Journal of metamorphic Geology*, **33**, 909–935, https://doi.org/10.1111/jmg.12153

Pownall, J.M., Hall, R., Armstrong, R.A. & Forster, M.A. 2014. Earth's youngest known ultrahigh-temperature granulites discovered on Seram, eastern Indonesia. *Geology*, **42**, 279–282, https://doi.org/10.1130/G35230.1

Rapp, R.P. & Watson, E.B. 1986. Monazite solubility and dissolution kinetics: implications for the thorium and light rare earth chemistry of felsic magmas. *Contributions to Mineralogy and Petrology*, **94**, 304–316.

Redler, C., White, R.W. & Johnson, T.E. 2013. Migmatites in the Ivrea Zone (NW Italy): Constraints on partial melting and melt loss in metasedimentary rocks from Val Strona di Omegna. *Lithos*, **190–191**, 1–12, https://doi.org/10.1016/j.lithos.2013.04.019

Rocha, B.C., Moraes, R., Möller, A., Cioffi, C.R. & Jercinovic, M.J. 2017. Timing of anatexis and melt crystallization in the Socorro–Guaxupé Nappe, SE Brazil: Insights from trace element composition of zircon, monazite and garnet coupled to U–Pb geochronology. *Lithos*, **277**, 337–355, https://doi.org/10.1016/j.lithos.2016.05.020

Rubatto, D. 2002. Zircon trace element geochemistry: partitioning with garnet and the link between U–Pb ages and metamorphism. *Chemical Geology*, **184**, 123–138, https://doi.org/10.1016/S0009-2541(01)00355-2

Rubatto, D., Hermann, J. & Buick, I.S. 2006. Temperature and bulk composition control on the growth of monazite and zircon during low-pressure anatexis (Mount Stafford, central Australia). *Journal of Petrology*, **47**, 1973–1996, https://doi.org/10.1093/petrology/egl033

Rubatto, D., Hermann, J., Berger, A. & Engi, M. 2009. Protracted fluid-present melting during Barrovian metamorphism in the Central Alps. *Contributions to Mineralogy and Petrology*, **158**, 703–722, https://doi.org/10.1007/s00410-009-0406-5

Rubatto, D., Chakraborty, S. & Dasgupta, S. 2013. Timescales of crustal melting in the Higher Himalayan Crystallines (Sikkim, Eastern Himalaya) inferred from trace element-constrained monazite and zircon chronology. *Contributions to Mineralogy and Petrology*, **165**, 349–372, https://doi.org/10.1007/s00410-012-0812-y

Schaltegger, U. 1994. Unravelling the pre-Mesozoic history of Aar and Gotthard massifs (Central Alps) by isotopic dating – a review. *Schweizerische Mineralogische und Petrographische Mitteilungen*, **74**, 41–51.

Schärer, U. 1984. The effect of initial $^{230}$Th disequilibrium on young U–Pb ages: the Makalu case, Himalaya. *Earth and Planetary Science Letters*, **67**, 191–204.

Schmid, S.M., Berger, A. *et al.* 1996. The Bergell Pluton (Southern Switzerland-Northern Italy): overview accompanying a geological-tectonic map of the intrusion and surrounding country rocks. *Schweizerische Mineralogische und Petrographische Mitteilungen*, **76**, 329–355.

Schmitz, S., Möller, A. *et al.* 2009. Chemical U–Th–Pb dating of monazite by 3D-Micro X-ray fluorescence analysis with synchrotron radiation. *European Journal of Mineralogy*, **21**, 927–945, https://doi.org/10.1127/0935-1221/2009/0021-1964

Schuster, R. & Stuewe, K. 2008. Permian metamorphic event in the Alps. *Geology*, **36**, 603–606, https://doi.org/10.1130/G24703A.1

Schuster, R., Scharbert, S., Abart, R. & Frank, W. 2001. Permo-Triassic extension and related HT/LP metamorphism in the Austroalpine-Southalpine realm. *Mitteilungen der Gesellschaft der Geologie und Bergbaustudenten in Österreich*, **45**, 111–141.

Spalla, M.I. & Marotta, A.M. 2007. P–T evolutions vs. numerical modelling: a key to unravel the Paleozoic to early-Mesozoic tectonic evolution of the Alpine area. *Periodico di Mineralogia*, **76**, 267–308, https://doi.org/10.2451/2007PM0029

Spalla, M.I., Zanoni, D., Marotta, A.M., Rebay, G., Roda, M., Zucali, M. & Gosso, G. 2014. The transition from Variscan collision to continental break-up in the Alps: insights from the comparison between natural data and numerical model predictions. *In*: Schulmann, K., Martínez Catalán, J. R., Lardeaux, J. M., Janoušek, V. & Oggiano, G. (eds) *The Variscan Orogeny: Extent, Timescale and the Formation of the European Crust*. Geological Society, London, Special Publications, **405**, 363–400, https://doi.org/10.1144/SP405.11

Spear, F.S. & Pyle, J.M. 2002. Apatite, monazite, and xenotine in metamorphic rocks, reviews in mineralogy and geochemistry, phosphates: geochemical, geobiological, and materials importance. *Reviews in Mineralogy and Geochemistry*, **48**, 293–335.

Stepanov, A.S., Hermann, J., Rapp, R.P. & Rubatto, D. 2012. Experimental study of monazite/melt partitioning with implications for the REE, Th and U geochemistry of crustal rocks. *Chemical Geology*, **300-301**, 200–220, https://doi.org/10.1016/j.chemgeo.2012.01.007

Stüwe, K. 1995. Thermal buffering effects at the solidus. Implications for the equilibration of partially melted metamorphic rocks. *Tectonophysics*, **248**, 39–51.

Todd, C.S. & Engi, M. 1997. Metamorphic field gradients in the Central Alps. *Journal of Metamorphic Geology*, **15**, 513–530.

Tribuzio, R., Thirlwall, M.F. & Messiga, B. 1999. Petrology, mineral and isotope geochemistry of the Sondalo gabbroic complex (Central Alps, Northern Italy): implications for the origin of post-Variscan magmatism. *Contributions to Mineralogy and Petrology*, **136**, 48–62.

Trommsdorff, V. 1966. Progressive Metamorphose kieseliger Karbonatgesteine in den Zentralalpen zwischen Bernina und Simplon. *Schweizerische Mineralogische und Petrographische Mitteilungen*, **46**, 431–460.

Vavra, G. & Schaltegger, U. 1999. Post-granulite facies monazite growth and rejuvenation during Permian to Lower Jurassic thermal and fluid events in the Ivrea Zone (Southern Alps. *Contributions to Mineralogy and Petrology*, **134**, 405–414.

Vielzeuf, D. & Holloway, J.R. 1988. Experimental determination of the fluid-absent melting reactions of pelitic rocks — consequences for the crustal differentiation. *Contributions to Mineralogy and Petrology*, **98**, 257–276.

Von Blanckenburg, F. & Davies, J.H. 1995. Slab breakoff. A model for syncollisional magmatism and tectonics in the Alps. *Tectonics*, **14**, 120–131, https://doi.org/10.1029/94TC02051

von Blanckenburg, F., Kagami, H. *et al.* 1998. The origin of Alpine plutons along the Periadriatic Lineament. *Schweizerische Mineralogische und Petrographische Mitteilungen*, **78**, 55–66.

Wenk, H.R., Wenk, E. & Wallace, J.H. 1974. Metamorphic mineral assemblages in politic rocks of the Bergell Alps. *Schweizerische Mineralogische und Petrographische Mitteilungen*, **54**, 507–554.

Whitney, D.L. & Evans, B.W. 2010. Abbreviations for names of rock-forming minerals. *American Mineralogist*, **95**, 185–187, https://doi.org/10.2138/am.2010.3371